The Non-Local Impacts of Antarctic Subglacial Runoff

Daniel N. Goldberg[1] ![ORCID], Andrew G. Twelves[1,2] ![ORCID], Paul R. Holland[3] ![ORCID], and Martin G. Wearing[1,4] ![ORCID]

[1]School of GeoSciences, University of Edinburgh, Edinburgh, UK, [2]Finnish Meteorological Institute, Helsinki, Finland, [3]British Antarctic Survey, Cambridge, UK, [4]European Space Research Institute, Frascati, Italy

Abstract Little is known about Antarctic subglacial hydrology, but based on modeling, theory and indirect observations it is thought that subglacial runoff enhances submarine melt locally through buoyancy effects. However, no studies to date have examined effects of runoff on sea ice and oceanography on the continental shelf. Here we use modeled and observational estimates of runoff to force a regional model of the Amundsen Sea Embayment. We find that runoff enhances melt locally (i.e., within the ice-shelf cavity), increasing melt at Thwaites ice shelf by up to 15 Gt/a given estimates of steady runoff, and up to 25 Gt/a if runoff is episodic as remote sensing measurements suggest. However runoff also has smaller non-local effects on melt through freshwater influence on flow and stratification. We further find that runoff reduces summer sea-ice volume over the continental shelf (by up to 10% with steady runoff but over 30% with episodic runoff). Furthermore runoff is much more effective at reducing sea ice than an equivalent volume of ice-shelf meltwater—due in part to the latent heat loss associated with submarine melting. Results suggest that runoff may play an important role in continental shelf dynamics, despite runoff flux being small relative to ice-shelf melting—and that runoff-driven melt and circulation may be an important process missing from regional Antarctic ocean models.

Plain Language Summary A number of floating ice shelves in Antarctica are exposed to warm waters which lead to strong melting, limiting shelves' ability to buttress against ice flow from the continent and also bringing warmed and freshened waters to the ocean surface—waters which in turn influence seasonal sea ice near the continent and insulate the deep ocean from the cold atmosphere. Meanwhile, large rivers under the Antarctic ice sheet carry melt from the ice sheet base to the ocean cavities beneath ice shelves. While a few studies have looked at the role these rivers play in ice-shelf melt, they do not examine the effects on ocean properties and sea ice in the open ocean. We find that these "rivers" not only amplify melting under ice shelves, but have far-reaching impacts on ocean circulation. We find that while the direct contribution of water from these subglacial rivers is small compared to that of ice-shelf melt, there is a disproportionate impact on seasonal sea ice.

1. Introduction

The ice shelves of the Amundsen Sea Embayment contribute several hundred gigatonnes of melt water per year to the ocean (Adusumilli et al., 2020). In addition to causing a loss of buttressing that can lead to sea level rise (Favier et al., 2014; Goldberg & Holland, 2022; Joughin et al., 2014; Seroussi et al., 2017), the flux of fresh water has impacts on the ocean as well. Ice-shelf melt drives upwelling of large volumes of Circumpolar Deep Water (CDW) and thinning of sea ice on the continental shelf (Jourdain et al., 2017)—the latter of which could have implications for biological production in seasonal polynyas (Arrigo et al., 2012). The addition of freshwater can stratify the ocean and also feed back on delivery of CDW to ice-shelf cavities (Bett et al., 2020; Kimura et al., 2017; Mathiot et al., 2017; Silvano et al., 2018).

Subglacial discharge at ice-shelf grounding lines is another source of fresh water. Like ice-shelf melt, it adds buoyancy at depth, which leads to upwelling of dense waters. At tidewater glaciers in Greenland and elsewhere, it is known that subglacial runoff leads to upwelling and strong melt at the terminus (e.g., Jenkins, 2011; Motyka et al., 2013; Slater et al., 2015), but also influences circulation within the fjord (Cowton et al., 2016; Slater et al., 2018). In Antarctica, subglacial runoff is observed to induce strong grounding-line melt and ice-shelf channel formation (Drews et al., 2017; Le Brocq et al., 2013), but few studies have attempted to quantify its impact on ocean physics. This is in part because comparatively little is known about Antarctic subglacial hydrology: little supraglacial melt is transported to the bed, melt is generated through frictional heating and geothermal flux (Van Liefferinge & Pattyn, 2013), and runoff is very poorly constrained. Still, Joughin et al. (2009) calculated subglacial melt values of 1.7 and 3.5 Gt/a for the catchments of Pine

Island and Thwaites glaciers, respectively, similar to annual runoff for large Greenland glaciers (Mernild et al., 2010a, 2010b). These mean values are small relative to ice-shelf melt, but observations of subglacial lake drainage suggest rates up to 50 Gt/a or more could be sustained for months (Malczyk et al., 2020; Smith et al., 2017). The transience and episodic nature of Antarctic subglacial runoff is further supported by direct observations of grounding-line discharge (Davis et al., 2023). It is therefore reasonable to ask how this runoff impacts submarine melt and ocean circulation, and how this varies with runoff magnitude and temporal character.

Nakayama et al. (2021) used a high-resolution model of Pine Island ice shelf cavity with a representation of runoff, in order to explain high satellite-observed melt rates which are not captured by models considering CDW-driven melt alone. Gwyther et al. (2023) use a regional model to show the role of runoff buoyancy in driving melt under Totten ice shelf and subsequent transport of the runoff tracer on the continental shelf. Importantly, these studies look primarily at local effects within the cavity where runoff is introduced. On the other hand, non-local effects of subglacial runoff, that is, its effects on sea ice, hydrography, and conditions in other ice-shelf cavities, have not been examined.

In this paper we apply modeled runoff from the catchments of Pine Island, Thwaites, Smith, and Getz glaciers to a regional sea ice-ocean-ice shelf model of the Amundsen Sea. The model is run for two decades; both time-constant and varying runoff scenarios are investigated. We focus both on local and non-local effects in our analysis. We find that runoff causes local increases in melt, consistent with other studies; but can influence melt in other ice shelves as well (both positively and negatively). We find also that runoff leads to a reduction of summer sea ice volume over the majority of the Amundsen continental shelf. It is seen that the effects of runoff on non-local melt are similar to that of ice-shelf melt in equivalent volumes; but that the effects on summer sea ice differ qualitatively from those of ice-shelf melt due to differences in the generation of subglacial and ice-shelf melt.

2. Methods

2.1. Regional Ocean Model

We model regional sea ice, ocean circulation and ice-shelf melt with the MITgcm (Losch, 2008; Losch et al., 2010; Marshall et al., 1997). The configuration is very similar to that of Naughten et al. (2022), which builds upon that of Kimura et al. (2017) and Bett et al. (2020). The domain extends from 140 to 70°W and 75.65–62.4°S, with resolution approximately 0.025° latitude (∼2.5 km) on the Amundsen shelf. Bathymetry and ice-shelf draft are interpolated from BedMachine Antarctica version 2 (Morlighem et al., 2020). Ocean-facing boundary conditions are sourced from the World Oceanographic Atlas (Locarnini et al., 2018; Zweng et al., 2019) and the B-SOSE state estimate (Verdy & Mazloff, 2017), and surface forcing is from ERA5. The Bear Ridge iceberg "wall" and iceberg freshwater flux from Bett et al. (2020) is used. Our model differs from that of Naughten et al. (2022) only in that rather than the Merino et al. (2016) iceberg freshwater flux, that of our model assumes a constant flux along the coastline. The impacts of this choice of iceberg flux were found to be negligible (K Naughten, pers. comm.), and so in this study we consider results of our **baseline** experiment (see below) to reflect those of Naughten et al. (2022).

Naughten et al. (2022) provides validation against available oceanographic and remotely sensed observations. Thermocline depth at Pine Island is captured well, but less so in front of Dotson ice shelf. Deep temperatures for both are underestimated post-2012 but well captured before. Temporal evolution and maximum extent of sea ice is well captured though summer extent is underestimated (the annual minimum has a negative bias of 64%). Inter-annual melt variability is well captured for Dotson and Pine Island, but Pine Island melt magnitude is slightly underestimated, especially in the late 2000s. Thwaites melt is low relative to Adusumilli et al. (2020), though there are no oceanographic estimates yet available to compare. Importantly, the tuning of this configuration did not take subglacial runoff into account. We refer below to this configuration as the **baseline**. For more detail on the configuration see Naughten et al. (2022).

2.2. Subglacial Runoff

In most of our experiments, our ocean model is forced with subglacial runoff. Our calculation of runoff volumes and locations is described here, followed by description of how runoff is implemented in the ocean model.
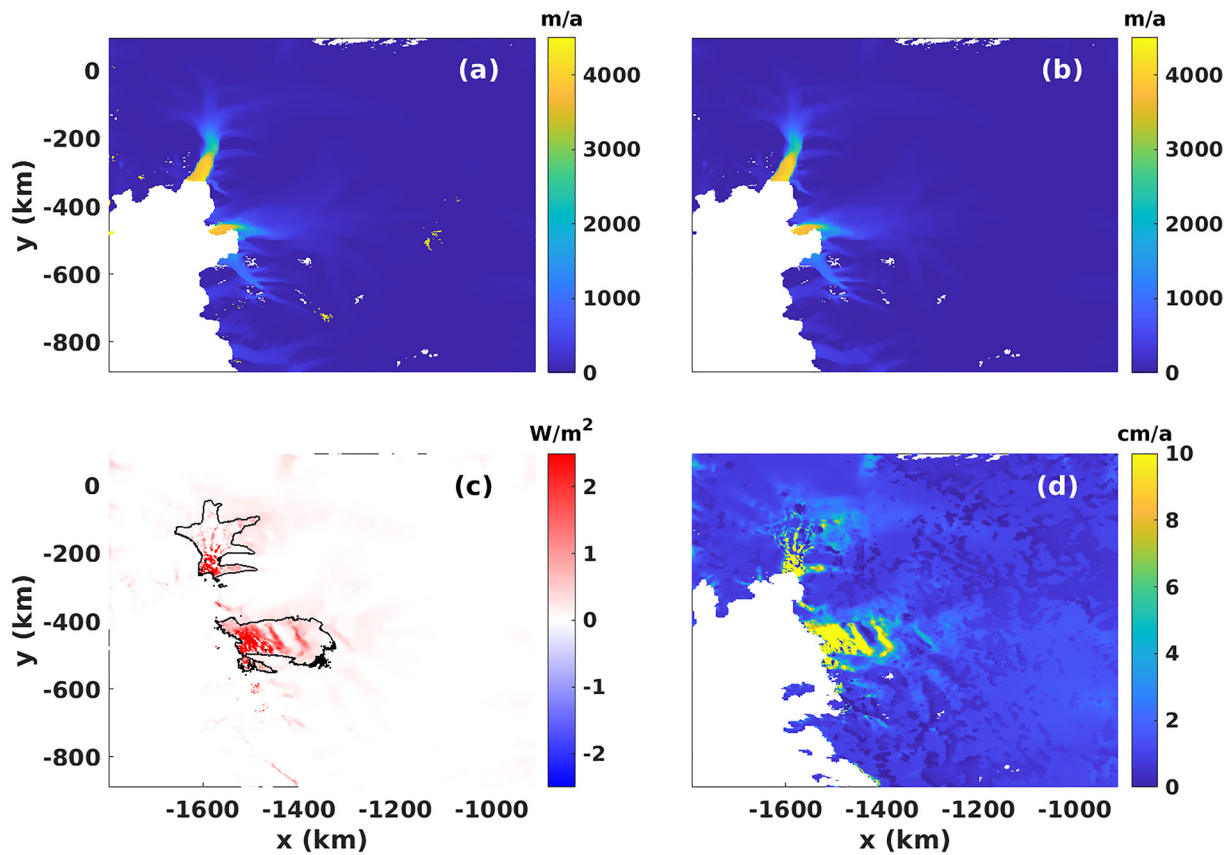
Figure 1. (a) Ice speed from the MEaSUREs data set within the model domain. (b) Modeled ice speed after inversion for basal friction and ice stiffness. (c) Frictional heating corresponding to the model solution in panel (b), where the black contours show regions of high speed for Thwaites and Pine Island. (d) Calculated melt rate in **runoff** experiment.

2.2.1. Melt Calculation

In order to provide an estimate of time-mean runoff at the grounding line, we first estimate the pattern of subglacial melt. To do so we solve the basal heat balance (e.g., Cuffey & Paterson, 2010; Joughin et al., 2009):

$$m_b = \frac{G + \tau_b u_b - k_i \Theta_i}{L_i \rho_i},$$ (1)

where m_b is basal melt rate, G is geothermal flux, k_i is thermal conductivity, Θ_i is ice basal temperature gradient, L_i is ice latent heat, ρ_i is ice density, and τ_b and u_b are basal drag and speed, respectively.

To calculate the frictional heating term $\tau_b u_b$, we use the ice-sheet model STREAMICE (Goldberg & Heimbach, 2013), which uses a higher-order approximation to Stokes flow and is capable of representing vertical shear as well as fast sliding flow regimes. To estimate $\tau_b u_b$ an inversion is carried out for basal drag and ice stiffness parameters. As described in Goldberg and Holland (2022), the stiffness parameter is initialized using a modeled temperature distribution (see below), and is allowed to vary though deviation from this initial distribution is penalized within grounded portions of the domain. The ice-sheet model is run at 2 km resolution over the Amundsen region (Figure 1), and the MEaSUREs (Rignot et al., 2011) Version 2 product, interpolated to the domain, constrains the inversion (Figures 1a and 1b). The resulting basal velocity and basal drag are then used to generate the frictional heating term (Figure 1c). Ice-sheet inversion requires specification of regularization parameters to prevent ill-posedness (Goldberg et al., 2019). The influence of these parameters on the model-observation fit was investigated, but they were found to have little impact on large-scale melt rates.

Heat flux from Martos et al. (2017) is used for G, with a topographic correction to account for small spatial scales (Colgan et al., 2021). STREAMICE does not have a thermomechanical component, therefore a modeled estimate
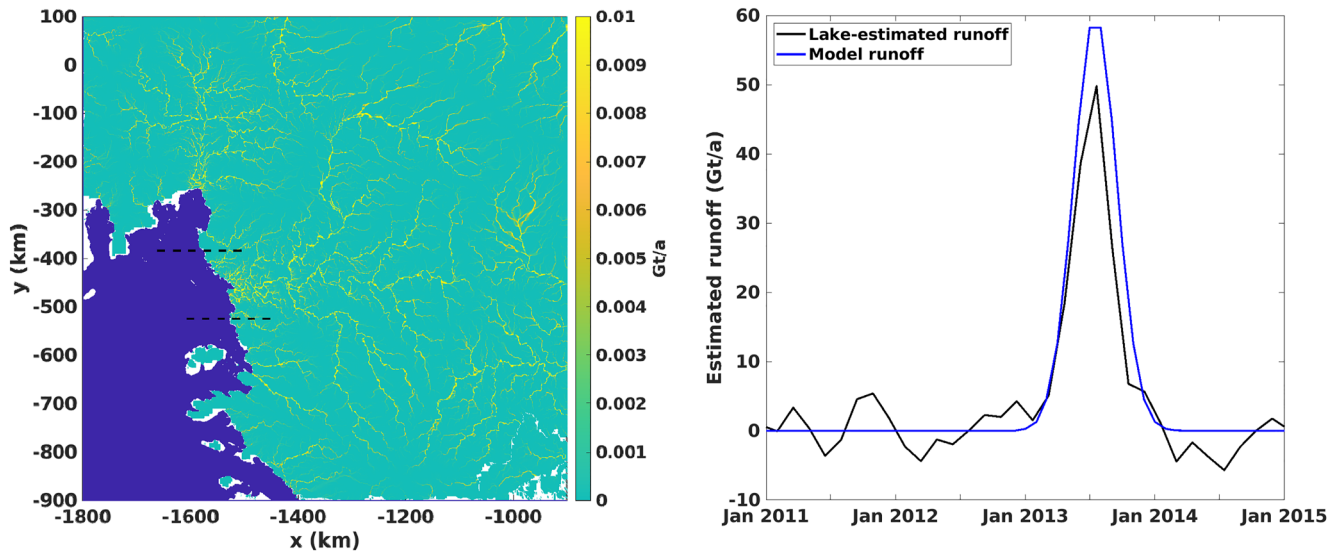
Figure 2. (a) Routing flux from Le Brocq et al. (2009) model calculation, with color range saturated to show entire network. Blue pixels represent ocean according to the BedMachine product, and white pixels are where the computation could not be carried out. The dashed black lines indicate the extent of the Thwaites grounding line in the **Thwaites only** and **time dependent runoff** experiments. (b) The runoff forcing for the **time dependent runoff** experiment. Black curve: combined rate of observed volume change under the four mapped lakes under Thwaites. Blue curve: a Gaussian profile which is an idealization of the observed change. The blue curve is zero prior to January 2013.

of ice temperature (Van Liefferinge & Pattyn, 2013) is used to calculate the vertical gradient, as well as for generation of the initial guess for ice stiffness. The vertical conduction term (Figure S1a in Supporting Information S1) is small relative to the geothermal heat flux (GHF) and frictional heating: the domain-integrated contribution of conduction is approximately 2×10^{11} W, which is approximately 10% of either dissipation or geothermal flux. Since geothermal flux (Figure S1b in Supporting Information S1) and dissipation are uniformly nonnegative and conduction is uniformly nonpositive, conduction accounts for approximately 10% of melt—meaning that even large errors in this term will have a small effect on overall melt and runoff at the grounding line. The calculated melt rate is shown in Figure 1d.

In a sensitivity experiment, the components of the above calculation are modified as follows: G and Θ_b remain the same, but frictional dissipation $\tau_b u_b$ is increased within the regions of fast flow of Pine Island and Thwaites (Figure 1c). Within each of the regions indicated, dissipation is increased uniformly by an amount equal to the mean frictional heating within that region. The rationale behind this experiment is that if there is a change in melt volume in the future, it will likely be due to a change in frictional effects rather than in geothermal flux. However, the imposed change in frictional heating is not based on ice-sheet projections, it is simply a means of assessing the impact of larger runoff.

2.2.2. Subglacial Routing

We use the routing model of Le Brocq et al. (2009) to determine the flux at the grounding line. Le Brocq et al. (2009) uses a laminar flow closure which relates subglacial flow velocity to background hydraulic potential, and uses this to derive a steady-state solution for subglacial flux. Subglacial flow is not coupled to water pressure in the model, and so modeled hydraulic potential depends only on ice thickness and bed elevation. The BedMachine Antarctica version 2 product (Morlighem et al., 2020) is used for these fields. Figure 2a shows the routing solution using the melt from Figure 1d.

2.2.3. Time Dependent Runoff

The above calculations generate a time-independent melt rate, intended to represent the average melt over long time periods. However, lake-drainage observations suggest that runoff is strongly time-varying. For time-dependent runoff, the time series of Malczyk et al. (2020) is used. The data describes volume change rates of 4 active lakes in the upstream part of Thwaites glacier. A time series of total volume loss is found by summing the contributions of all lakes. The result (Figure 2b) shows intra-annual variability on the order of 3–5 Gt/a over the 2011–2015 period, but the most noticeable feature is a pulse of up to 50 Gt/a that lasts for about 1 year (2013–2014).

In the experiment forced by time-dependent runoff, an assumption is made that the water which collects in these lakes is mainly drainage from the upstream, slower-flowing parts of the catchment where there is relatively little frictionally driven heating. Thus, we partition runoff into a steady component, driven by frictional heating and thermal conduction alone; and a time-dependent component. The steady component is found simply by setting GHF to zero and routing the melt as described above. For the time-dependent component, the runoff flux is set to zero for all cells away from the Thwaites grounding line (dashed lines in Figure 2a), and flux along the grounding line is scaled so that the total flux (for the time-dependent component) follows the idealized time series in Figure 2b. In other words, there is a steady runoff along the grounding line of the domain corresponding to frictional heating only, and from 2013 to 2014 there is an additional pulse representing lake drainage.

2.3. Implementation of Runoff in Ocean Model

In order to implement runoff within MITgcm, the grounding line runoff from the routing product described above is first interpolated to the ocean grid. The grid of the routing model is in polar-stereo coordinates with 500 m resolution, and the ocean grid is in latitude/longitude coordinates with an approximately 2.5 km resolution, so the grounding line of the ocean model does not perfectly align with the edge of the routing domain. Runoff is therefore interpolated as follows. The output of the routing model is a gridded field which contains volumetric fluxes (in m³/s) that represent the flux coming out of each cell. Cells where the routing network terminates are identified. For each one of these cells, the flux is added to the nearest nonempty ocean column, generating a 2D field which is used to force the ocean model.

The runoff is assumed to enter the ocean with zero salinity and to be at the pressure-depressed freezing point. At each time step of the ocean model, in columns with nonzero grounding line flux as determined by the process above, the salt and temperature tendency in the deepest ocean cell are thus updated according to this flux value:

$$\frac{dS_{i,k}}{dt} = \frac{Q_i(0 - S_{i,k})}{A_i h_k},$$ (2)

$$\frac{dT_{i,k}}{dt} = \frac{Q_i(p_{i,k}b - T_{i,k})}{A_i h_k},$$ (3)

where i refers to the column, and k to the depth level, of the bottom cell; $S_{i,k}$, $T_{i,k}$, and $p_{i,k}$ are the salinity, temperature, and pressure, respectively, of the cell at the current time step; Q_i is the flux into the column; and b is the freezing point dependence on pressure (set to -7.61×10^{-4}°C per dbar). Where the bottom cell is below a minimum thickness (in this study 40 m), the tendency is distributed over the bottom two cells in a conservative fashion similar to the under-ice shelf boundary layer treatment of Losch (2008), in order to prevent overly strong freshening and cooling. The above changes are made to MITgcm version 67v.

The treatment does not affect ocean momentum (velocities)—this is in contrast to Nakayama et al. (2021) and Slater et al. (2015), which implement runoff through open boundary conditions. However, given the low resolution of the model, this impact is likely to be small.

2.4. Ice-Shelf Cavity Overturning

In the analysis of sea-ice response to runoff, rates of volumetric overturning under the Amundsen ice shelves are calculated. In this calculation the horizontal convergence of flow below a certain depth is taken as a proxy for overturning. Convergence is calculated by integrating horizontal convergence of velocity at each depth layer underneath the ice shelf, giving the net flux per unit depth leaving the cavity at that depth level. This quantity is then integrated vertically up to a certain depth, chosen as the depth for each ice shelf below which there is predominantly inflow of warm water. This depth is chosen as 600 m for Thwaites and 550 m for Pine Island (Figure S2 in Supporting Information S1).

2.5. Experiments

Table 1 summarizes the experiments carried out in our study. We refer to the ocean simulations forced by the two steady runoff cases as the **runoff** and **hi runoff** experiments, and to the run forced by lakes data as **time dependent runoff**. An additional experiment, **Thwaites only**, is carried out where runoff is as in the **runoff** experiment, but set to zero away from the Thwaites grounding line (see dashed lines in Figure 2a). Additionally, we consider two scenarios without runoff but where melt rates are modified by changing c_{fric}, the drag coefficient governing

Table 1
A Listing of All Experiments Carried out in This Study, in Terms of Steady and Time-Dependent Runoff Forcing and Modification of Melt Parameters

Experiment	Steady runoff component	Time-Dep. Runoff component	Modified c_{fric}
Baseline	—	—	—
Runoff	domain	—	—
Hi runoff	increased $\tau_b u_b$	—	—
Time dependent runoff	$\tau_b u_b$ only	Malczyk et al. (2020)	—
Thwaites only	Thwaites catchment only	—	—
Increased c_{fric}	—	—	0.0055 (PIIS, TIS, DIS/CrIS only)
Increased Thwaites c_{fric}	—	—	0.01 (TIS only)

ice shelf basal melting (Dansereau et al., 2014). In **increased c_{fric}**, this value is increased from 0.004 to 0.0055, but only under Pine Island, Thwaites and Dotson/Crosson ice shelves. The purpose of this experiment is to assess the sensitivity of shelf conditions and sea ice response to freshwater sourced from ice shelf melting as opposed to subglacial runoff. Specifically, the value of c_{fric} is chosen so that the combined time-mean melt increase for Pine Island, Thwaites and Dotson/Crosson (relative to **baseline**) is similar to the increase in fresh water discharge (runoff and melt) from these ice shelves in the **runoff** experiment. The frictional coefficient of Getz ice shelf is left unchanged in this scenario due to its low sensitivity to runoff (Section 3.1). The **increased Thwaites c_{fric}** experiment is similar, but here c_{fric} is modified only under Thwaites ice shelf (from 0.004 to 0.01), with the purpose of investigating freshwater effects on cavity stratification as a function of water source. Each experiment is run for 20 years from 1 January 1995 to 31 December 2014, beginning from the saved state of the baseline run. A freshwater tracer for combined runoff and ice-shelf melt is implemented in the **baseline** experiment.

In the **runoff** experiment, the majority of the runoff enters the Amundsen through three large channels beneath Thwaites and Pine Island glaciers (Figure 3). The total runoff across the Thwaites and Pine Island grounding lines are approximately 4.6 and 2.7 Gt/a, respectively. These values are larger than those cited in Joughin et al. (2009), though this could result from the use of a different GHF estimate (Joughin et al. (2009) used a constant value for GHF), a more recent velocity estimate, or both. In **hi runoff** these increase to 6.8 and 3.9 Gt/a, respectively. Meanwhile, at most 0.4 Gt/a enters from each of the Dotson/Crosson and Getz grounding lines. In **time dependent runoff**, runoff reaches nearly 50 Gt/a, but only for a few months (Figure 2b).

Examination of the freshwater tracer in the **baseline** experiment shows a domain-mean concentration that rises steadily to ∼6% from 1995 to 2003, after which it varies by less than 10% (Figure S3 in Supporting Information S1).
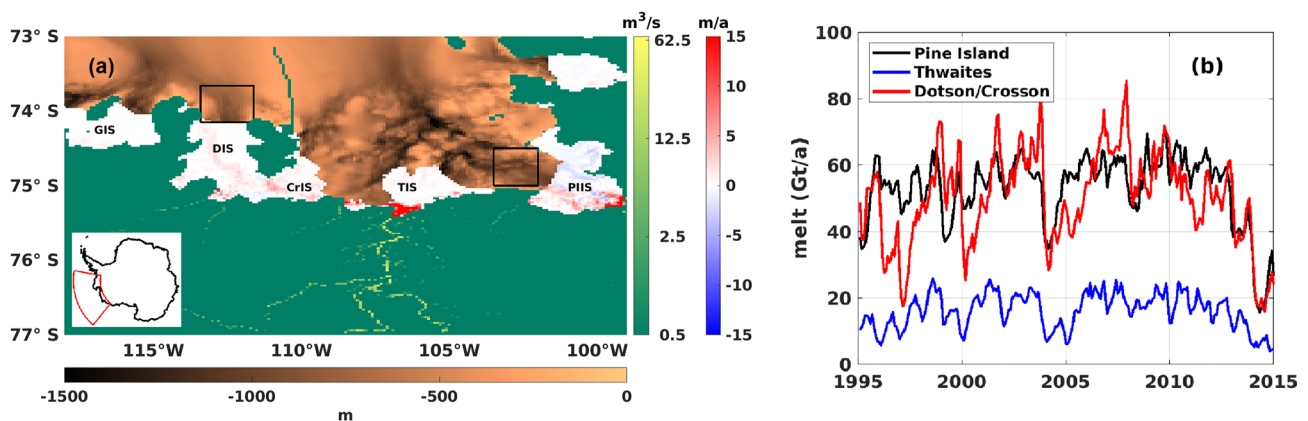
Figure 3. (a) A subset of the model domain containing the continental shelf and modeled ice shelves (full domain is given in the inset), with ocean bathymetry as copper shading. Red-blue shading shows the time-mean change in melt in the **runoff** experiment relative to **baseline**. Where ice is grounded, the routing solution corresponding to the **runoff** experiment is shown on a logarithmic (green-yellow) scale. The black boxes indicate the regions used for the Hovmöller diagrams in Figures 6 and 7. Relevant ice shelves are identified (GIS: Getz; DIS: Dotson; *CrIS*: Crosson; TIS: Thwaites; PIIS: Pine Island. The green line extending from the island between DIS and CrIS is the Bear Ridge iceberg "wall" from Bett et al. (2020). (b) Time series of monthly melt rate corresponding to Pine Island, Thwaites, and Dotson/Crosson ice shelves in the **baseline** run.

It is inferred that the adjustment time of the system to the input of a tracer (such as freshwater runoff) is approximately 8 years. Therefore any "non-local" effects of runoff on melt may not be fully realized until after this time, whereas the response of melt to "local" runoff is much faster (Nakayama et al., 2021). Therefore, in our study "local" impacts of runoff on ice-shelf melt and overturning are analyzed for the full 1995–2015 period, whereas "non-local" effects on ice-shelf melt, and sea-ice and ocean characteristics on the continental shelf, are analyzed over the 2003–2015 period. In the **time dependent runoff** experiment, which is inherently transient, there is no assumption of adjustment to the episodic runoff.

2.6. Limitations of Approach

The inclusion of subglacial runoff in a three-dimensional ocean model of ice-ocean interaction is relatively new; only a handful of studies have done so (e.g., Cowton et al., 2016; Gwyther et al., 2023; Nakayama et al., 2021; Slater et al., 2015). Thus we consider the assumptions and potential limitations in our approach. Here we limit our discussion to how we represent transport of subglacial water underneath the ice sheet, and its introduction to the cavity at the grounding line.

As discussed above, a routing approach is used to assess transport of melt to the grounding line. This routing model takes a very simplistic view of subglacial hydrology. In reality, ice-sheet subglacial flow exhibits distributed and channelized regimes, and effective pressures which depend on both subglacial flux and ice-sheet dynamics (Brinkerhoff et al., 2021; Nienow et al., 2017), and a model which resolves these processes might be necessary to fully represent the subglacial environment of Amundsen ice streams. We note that grounding line flux in our **runoff** experiment compares well with a recent study of Thwaites using a more sophisticated model of hydrology (Hager et al., 2022). Our calculated grounding line flux (4.6 Gt/a) is within the range found by their study, and exits at a similar location (their Figure 5). Still, we emphasize that our routing model does not give a complete picture of the subglacial environment.

The design of our **time dependent runoff** experiment implicitly assumes a one-to-one correspondence between lake drainage and runoff. This is unlikely due to transit time, subglacial storage, and the potential for unobserved lakes or drainage out of the Thwaites catchment. It also neglects additional subglacial melt due to frictional heating associated with channelized flow. Very little is still known about the Antarctic subglacial environment, and our representation captures to leading order the evidence that areas close to the grounding line exhibit efficient drainage (Hager et al., 2022; Schroeder et al., 2013). Still, it should be kept in mind that the runoff response to lake drainage may be lagged or muted—neither of which is represented here—and that the contribution may be larger or smaller than that considered.

Finally we emphasize that neither the **runoff**, **hi runoff** nor the **time dependent runoff** forcings are intended as the "correct" representation of subglacial runoff in a spatial or temporal sense. Rather, we present our scenarios as end-members representing time-constant and episodic modes of runoff. Furthermore, our model resolution may be too coarse to capture detailed melt patterns of ice-shelf melt response to runoff and near the grounding line (Holland et al., 2023; Nakayama et al., 2021). Our focus is rather on the hydrographic impacts of runoff within and externally to ice-shelf cavities, and the influence they have on ice-shelf melt and sea-ice reduction.

3. Results

3.1. Ice-Shelf Melt

We center our discussion around the high-melting ice shelves in the Amundsen Sea, namely Pine Island, Thwaites, and Dotson and Crosson (or Dotson/Crosson). Figure 3a shows the additional melt under these shelves in the **runoff** experiment, relative to **baseline**, averaged over the 20-year run. The strongest melt impacts appear close to subglacial inputs (as seen from comparison with routing results)—although as mentioned in Section 2.6, care should be taken in drawing inference from spatial melt patterns in such a coarse model. Melt time series from **baseline** are shown in Figure 3b. Pine Island and Dotson melt are similar to shipboard observations (Naughten et al., 2022), but Thwaites melt rates are much lower than other published results, which are in the range of 70–80 Gt/a for modeling studies (Holland et al., 2023; Serussi et al., 2017) and 60–100 Gt/a for satellite studies (Adusumilli et al., 2020; Depoorter et al., 2013; Rignot et al., 2013).

Figure 4 shows melt increase relative to **baseline** melt for the other experiments under the various ice shelves. Here and in Section 3.2, results are presented as percent anomalies rather than absolute change. Of all shelves,
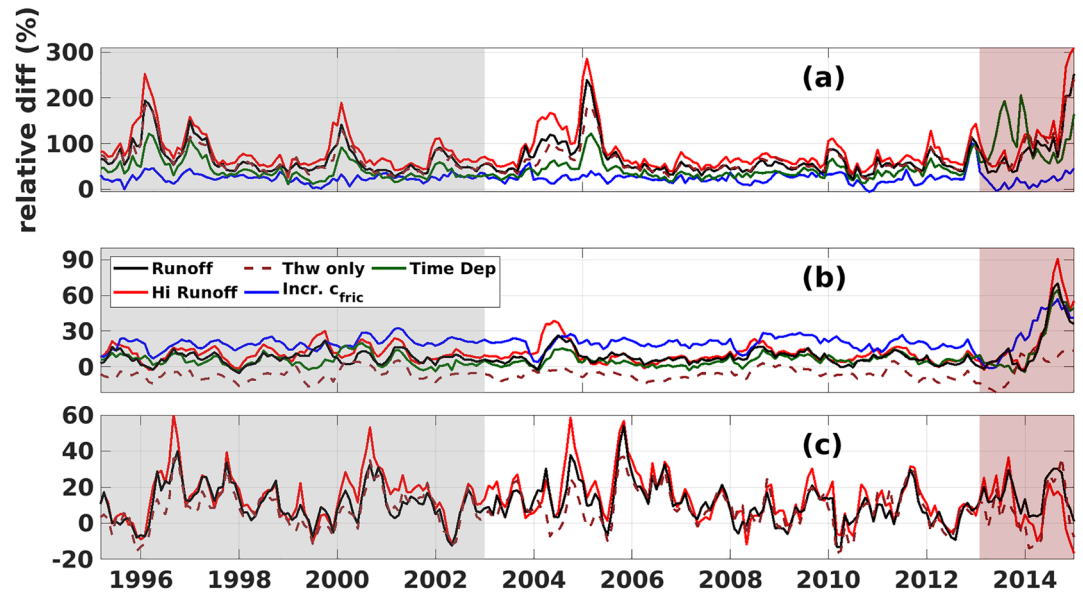
Figure 4. Monthly difference in melt relative to the **baseline** experiment, shown in per cent, for the perturbation experiments under (a) Thwaites, (b) Pine Island, and (c) Dotson/Crosson. Gray shaded regions represent the "spinup" period over which the continental shelf adjusts to freshwater input, and the red shaded regions indicate where runoff in the **time dependent runoff** experiment does not include the lake drainage. Only the **runoff**, **hi runoff**, and **Thwaites only** experiments are shown for Dotson/Crosson. Note the differing scales of the y-axes.

Thwaites sees the strongest proportional response in the **runoff** experiment due to its low baseline melt (Figures 3b and 4a). There is a marginal increase when runoff is increased in **hi runoff**, and similar is seen for Pine Island (Figure 4b). Note that the relative responses in Thwaites and Pine Island are very large in 2014–15, but this is due to the low melt rates in **baseline** in this year.

At Dotson and Crosson shelves, the melt increase in **runoff** is substantial (reaching 20% in most years and sometimes much more), considering the relatively small runoff input (Figure 4c). From the **runoff** results it is difficult to attribute increased melting at Dotson/Crosson to either locally (within the cavity) or non-locally sourced runoff. However, in the **Thwaites only** experiment, where runoff is released only from Thwaites, the melt anomalies under Dotson/Crosson are very similar to those in **runoff**. Meanwhile, the melt under Pine Island is slightly decreased relative to **baseline**. In the **time dependent runoff** experiment, when the runoff reaches its peak in summer 2013, the Thwaites melt anomaly is approximately 2.5 times that of the **runoff** experiment—though at the same time, runoff is nearly an order of magnitude larger. The other ice shelves' melt response to this episodic runoff is minimal.

Getz ice shelf is another high-melting ice shelf in the Amundsen—however, melt anomalies under Getz are small in the perturbation experiments, and so we do not include results for Getz in Figures 3b and 4. We also do not plot results from the **time-dependent runoff** and **increased c_{fric}** experiments for Dotson/Crosson so that the effects of increasing runoff and allowing only Thwaites runoff can be seen more clearly. We present results from all ice shelves, and all experiments, in Figure S4 and S5 in Supporting Information S1.

3.2. Sea Ice

We examine the effects of ice-shelf freshwater fluxes (both runoff and melt) on effective sea ice thickness, the volume of sea ice per unit area within a grid cell. In this analysis we predominantly compare the **increased c_{fric}** and **runoff** experiments. In terms of combined freshwater anomaly from Pine Island, Thwaites and Dotson/Crosson between 2003 and 2015, there is a moderate correlation between the experiments (0.54), and the means differ by ~6%. (As mentioned in Section 2.5, 1995–2003 is considered spinup from the perspective of sea ice influence).

We examine sea ice on the continental shelf only. Although the model domain extends far beyond the shelf, sea ice cover on-shelf is particularly important because it affects surface processes which could have impacts on CDW properties at depth; and in the spring and summer months it controls the light available for photosynthesis. Figure 5a shows mean ice thickness anomalies relative to the **baseline** run over a region with depth less
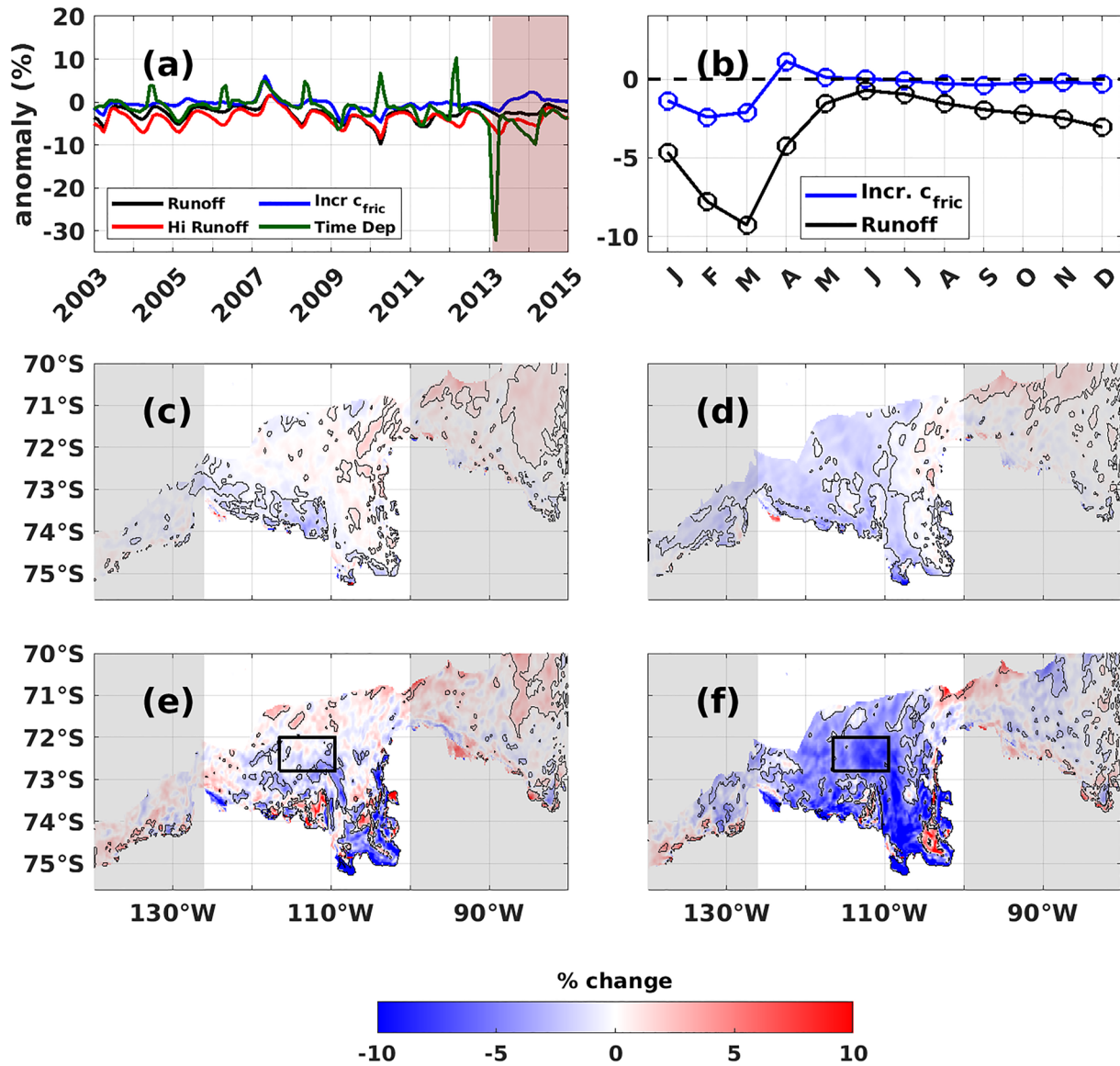
Figure 5. (a) Monthly change in mean effective sea ice thickness on the continental shelf, relative to **baseline**, in the experiments shown. The ocean-model spinup period is excluded, and the red-shaded period indicates where time-dependent runoff is nonzero. Results in panels (b)–(f) correspond to the period shown. (b) A monthly climatology for 2003–2015 of mean effective sea ice thickness relative to **baseline** in the **runoff** and **increased** c_{fric} experiments. (c) Change in winter (JJA) sea ice effective thickness relative to **baseline** in the **increased** c_{fric} experiment. Black contours indicate 95% significance, based on a *t*-statistic with degrees of freedom equal to the number of months. (d) Similar to (c) for **runoff**. Panels (e), (f) similar to panels (c), (d) for summer sea ice thickness.

than 1,500 m between 125 and 100°W (the approximate zonal extent of the summer ice-free region in Naughten et al., 2022). Averaged over the 2003–2015 period, the sea ice anomalies for the both **runoff** and **increased** c_{fric} are negative, but mean sea ice thinning in **runoff** is larger (2 cm vs. 3 mm). Overall the **runoff** anomaly is the most negative in summer, again with greater losses than **increased** c_{fric}. This is made clearer by examining a climatology of mean sea ice thickness anomaly for both experiments (Figure 5b). In the winter (June/July/August, i.e., JJA) months, the climatological area-averaged thinning is similar between the two experiments, and is relatively small. In the spring (September/October/November, i.e., SON) and summer (December/January/February, i.e., DJF) months, the climatologies diverge, with larger thinning in the **runoff** experiment.

The behavior exhibited in Figure 5b is explored further in Figures 5c–5f, which show spatial patterns of sea ice anomalies for each experiment, averaged over winter (Figures 5c and 5d) and summer (Figures 5e and 5f) months, respectively. As expected from Figure 5b the winter thinning is relatively small for both **increased** c_{fric}
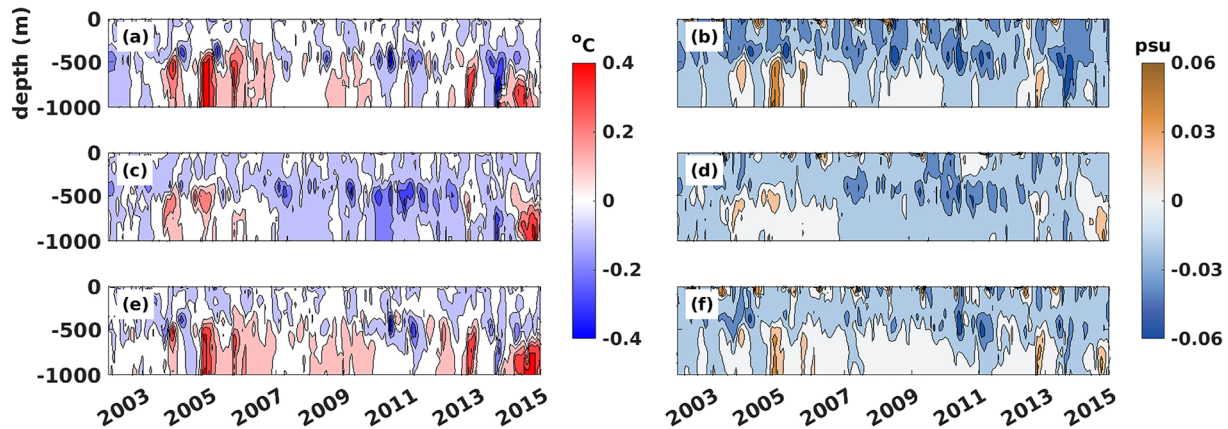
Figure 6. Left column: Hovmöller diagrams of temperature anomaly at depth relative to the **baseline** experiment, width-averaged over the box at the Dotson front in Figure 3a, for the (a) **runoff** experiment, (c) **increased c$_{fric}$** experiment, and (e) **Thwaites only** experiment. Right column: as in the left column but for salinity.

(Figure 5c) and **runoff** (Figure 5d). In the summer months, thinning is mostly localized around the coast in the **increased c$_{fric}$** experiment (Figure 5e). Meanwhile, there is fairly large thinning in the **runoff** experiment (Figure 5f): ∼10% over most of the continental shelf, which amounts to 5–10 cm.

Jourdain et al. (2017) examined the impact of ice-shelf melt on sea ice across an ensemble of experiments with different ice-shelf melt parameters (their Figure 10b). Their result is qualitatively similar to the patterns in Figures 5c and 5e, with strong thinning close to the coast. However, theirs was an annual result, and also used a different ocean model and a different experimental design, so it is not a straightforward comparison. Still, our results suggest that freshwater sourced subglacially has a qualitatively different effect on sea ice than water sourced from submarine melt. In the discussion below we explore potential reasons for this.

While our main focus in this section and in the discussion below is on how equal volumes of subglacial runoff and submarine melt can have potentially differing impacts, we briefly note that Figure 5a also shows sea-ice impacts in the **time dependent runoff** experiment. The effect is quite strong, but only for a single season when subglacial runoff is at its peak. The results suggest that episodic runoff can have significant, but short-lived, effects on sea ice thickness.

4. Discussion

4.1. Ice-Shelf Melt

In the **hi runoff** experiment, runoff from Thwaites is approximately 50% larger than in **runoff**, while the melt perturbation increases by 28% (s.d. 14%). At the same time, in **time dependent runoff**, the runoff at its largest is ∼13 times larger than in **runoff**, while the summer 2013–2014 melt rate is increased by a factor of 2.5.
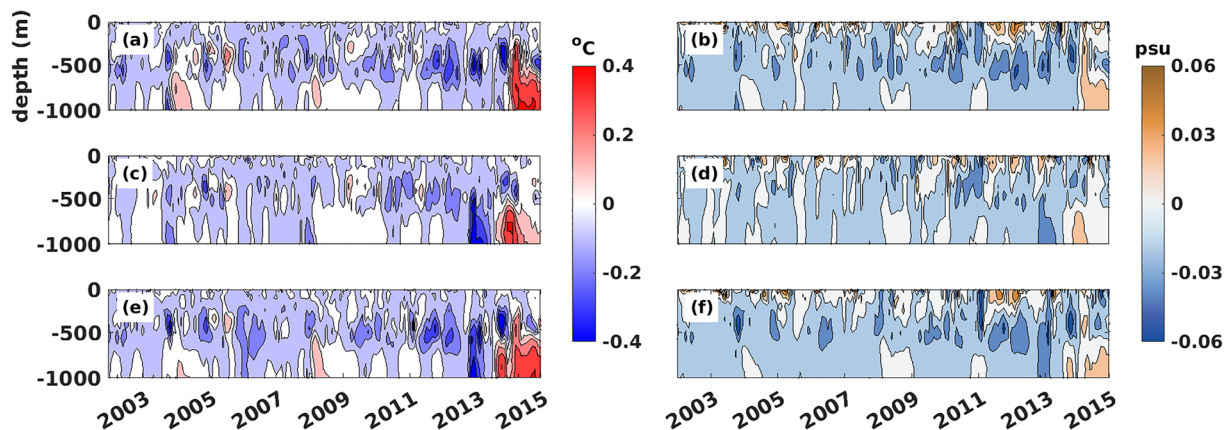
Figure 7. As in Figure 6, but for the Pine Island ice shelf front box in Figure 3a.

These results are qualitatively similar to theoretical and modeling studies of runoff-forced plume melting at tidewater glaciers (Cowton et al., 2015; Jenkins, 2011; Slater et al., 2015; Xu et al., 2013), which find sub-linear dependence of melt on runoff flux. The theoretical results of Jenkins (2011) come from an idealized model of small-scale processes near the grounding line, however, whereas we are considering cavity-integrated melt within a large-scale, sophisticated ocean model, so a rigorous comparison cannot be made.

For the majority of the time period studied, Pine Island and Dotson/Crosson ice shelves exhibit melt responses of similar magnitude in the **runoff** experiment (Figures 4b and 4c), despite an order of magnitude difference in runoff flux at their respective grounding lines. This suggests a "non-local" influence of runoff on the Dotson/Crosson ice shelves. The idea is reinforced by the **Thwaites only** experiment, which leads to a very similar response in melt rates under Dotson/Crosson even when there is zero runoff at the Dotson and Crosson grounding lines (Figure 4c). The elevated melt under Dotson/Crosson in **runoff** is likely due to a warm anomaly found at depth at the Dotson ice-shelf front (Figure 6a), where temperatures below 500 m are increased up to 0.4°C relative to **baseline**. The warm anomaly is not steady, but exhibits strong seasonal and interannual variability. Meanwhile there is freshening of 0.02–0.04 g/kg above 500 m (along with a slight cooling), with comparatively little change in salinity at depth (Figure 6b).

The warming at depth coincident with surface freshening suggests a mechanism where increased stratification prevents surface-driven cooling of CDW. Bett et al. (2020) showed that freshwater fluxes from icebergs (crudely represented as an ocean surface freshwater flux) can increase stratification and prevent cooling of CDW due to surface processes at Dotson ice shelf—and freshwater sourced from either distal runoff and/or increased ice shelf melt may play a similar role. The warming effect at depth therefore depends not only on freshwater flux but on surface forcing and how strongly the column is preconditioned for deep mixing, both of which vary interannually.

Meanwhile, the **increased c_{fric}** (Figures 6c and 6d) and **Thwaites only** (Figures 6e and 6f) experiments also show surface freshening and episodic warming at depth. In each case the freshening is less extensive, as is the warming (**runoff** and **Thwaites only** both show intermittent warming between 2009 and 2013 while **increased c_{fric}** shows mild cooling). Still, both experiments reinforce the influence of stratification on the presence of CDW in the Dotson cavity.

At the front of Pine Island, and aside from isolated periods, warming at depth is largely absent in the **runoff** and **increased c_{fric}** experiments (Figures 7a and 7c, respectively). In fact, there is cooling in some years. Therefore, although Pine Island melt increases in the **runoff** experiment, it is unlikely this is attributable to deep warming (with the exception of 2013–2014, discussed below), but rather that melt is locally runoff-forced. Cooling at depth is seen in **Thwaites only** as well, and could be the cause of the negative Pine Island melt anomaly in that experiment, which is not "hidden" by a local runoff source.

The most pronounced warming at depth for Pine Island (∼0.4°C) is seen in 2013–2014. During this period there is a cool bias with respect to observations in **baseline**, which is attributed to convection by Naughten et al. (2021). The warming relative to **baseline** is likely responsible for the increase in melt seen in the runoff experiments, and **increased c_{fric}** as well. It is possible that, similarly to Dotson, surface freshening due to runoff and/or melt increases stratification and prevents the strong surface-driven cooling of CDW that occurs during this time in **baseline**. The 2013–2014 warming is seen in the **runoff**, **Thwaites only** and **increased c_{fric}** experiments (Figures 7a, 7c, 7e), suggesting that it is driven by freshwater flux regardless of the source.

It is not clear why runoff forcing at Thwaites would drive a cooling at depth in front of Pine Island. Yoon et al. (2022) show evidence of a double-gyre system of circulation in front of Pine Island ice shelf which controls the conditions within the cavity, and argue that a change in the position of the calving front can alter this double-gyre pattern and hence the cavity conditions. It is possible that fresh water input from Thwaites ice shelf can impact this double-gyre circulation as well, but further investigation is needed.

4.2. Sea-Ice Reduction

The above discussion of non-local effects of runoff on ice-shelf melt suggests impacts of runoff on hydrography are due to their contribution to fresh water fluxes—such that, for instance, an increase in ice-shelf melt may have similar effects to a runoff increase of similar magnitude. This does not appear to be the case for sea ice, as an increase in freshwater flux due to runoff has a bigger effect on summer sea ice than a much larger increase due to melt alone (cf. Figure 5).
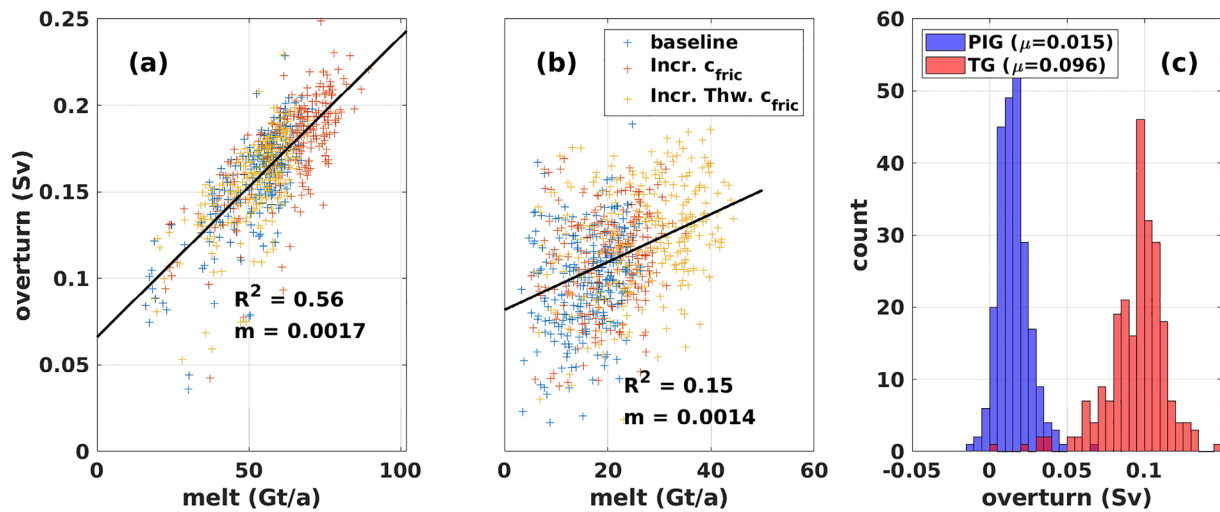
Figure 8. (a) Plot of calculated overturning versus ice-shelf melt for Pine Island in the non-runoff experiments. Each data point represents a different month between 1995 and 2015. (b) Similar to (a) for Thwaites. (c) Histograms of increase in overturning (relative to **baseline**) for Pine Island and Thwaites in the **runoff** experiment. The samples represent monthly values between 1995 and 2015.

### 4.2.1. Influence on Overturning

Jourdain et al. (2017) suggest that increased overturning in response to elevated melt can bring more heat to ice-shelf fronts, where it is brought to the surface through mixing and vertical advection. We investigate the relationships between melt rates and overturning, and between runoff and overturning, under Pine Island and Thwaites ice shelves. Similar to our assumption regarding adjustment of melt, we assume overturning response time to melt is fast. As such, monthly melt rates and overturning are compared using combined output from all non-runoff experiments (Figures 8a and 8b). In the **runoff** experiment, runoff is constant, and so overturning response is assessed by finding the difference between experiments in all months, and analyzing the resulting distribution (Figure 8c).

For Pine Island, we see increased overturning in response to both melt and runoff (Figures 8a and 8c). Moreover the responses are similar in terms of overturning per unit of freshwater flux: in the non-runoff experiments, the best-fit linear relationship between melt and overturning yields a slope $m = 0.0017$ Sv per Gt/a of melt ($R^2 = 0.56$). In the **runoff** experiment, the mean 1995–2015 increase of Pine Island melt relative to **baseline** is about 4 Gt/a, giving a combined release of ~7 Gt/a released into the cavity (runoff plus additional melt). From the above melt-overturning relationship, the predicted increase in overturning in **runoff** is thus ~0.012 Sv, whereas an increase of 0.014 Sv is seen (Figure 8c). In the Thwaites cavity there is a weak relationship between melt and overturning (Figure 8a; $m = 0.0014$, $R^2 = 0.15$), and a calculation similar to the above predicts an increase in ~0.02 Sv in response to the presence of runoff. Meanwhile, a mean increase of ~0.1 Sv is seen (Figure 8c).

The above comparisons suggest that, for the Pine Island cavity, the response in overturning is agnostic to the source of fresh water; while under Thwaites, runoff has a distinct effect on overturning. The reasons for this are unclear. It could be that under Pine Island, the runoff and its induced melt is a relatively small perturbation to the background state, which is not the case for Thwaites, hence the qualitatively different response. Further investigation of the mechanism of overturning, with a range of model types and resolution, is needed.

Nevertheless, we examine the effects of this increased overturning—and the associated heat transport to the upper ocean—on temperatures in the upper 400 m, averaged over the region indicated by the mid-shelf rectangular box in Figures 5e and 5f. This region is chosen because of its alignment with the Amundsen Polynya, which supports extremely high rates of productivity in summer months due to the relative availability of light (Yager et al., 2012). The results are presented as a Hovmöller diagrams for the **runoff**, **increased** c_{fric}, and **Thwaites only** experiments (Figures 9a, 9c, and 9e, respectively). In the runoff experiment, there is a strong seasonal surface warming (relative to **baseline**) that extends down to ~50–100 m in most years, as well as a periodic warming of approximately 0.1°C which extends from ~100–400 m. The strong surface warming is likely due to increased radiative heating
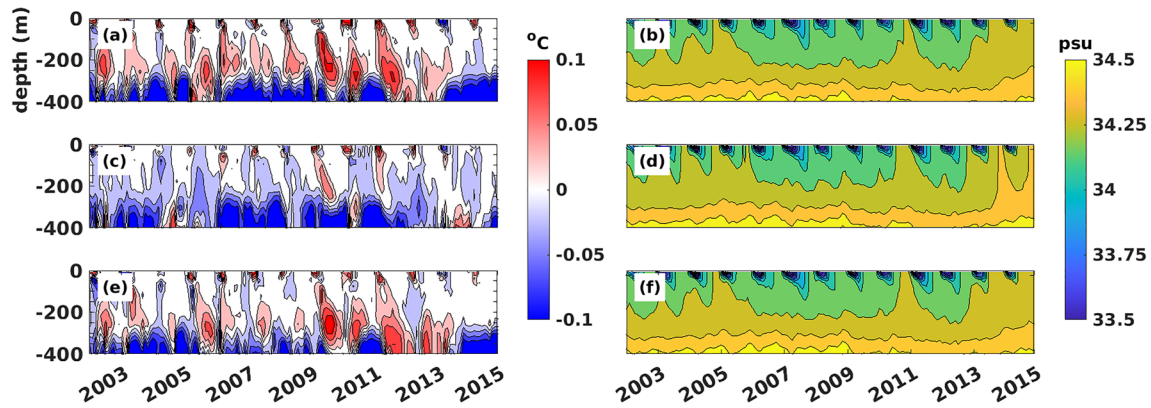
Figure 9. Left column: Hovmöller diagrams of temperature anomaly at depth relative to the **baseline** experiment, width-averaged over the box on the continental shelf in Figures 5e and 5f, for the (a) **runoff** experiment, (c) **increased** c_{fric} experiment, and (e) **Thwaites only** experiment. Right column: as in the left column but for salinity.

from reduced sea ice cover, and as such is a result rather than a cause of lowered sea ice. The deeper warming, on the other hand, likely arises from upwelling and export of CDW from within the ice-shelf cavity, rather than vertical mixing. It can be seen from salinity Hovmöller diagrams for the same location (Figures 9b, 9d, and 9e) that vertical mixing of seasonal surface freshening does not extend to these depths; rather, winter mixing erodes the signal at depth.

We propose that relatively warm waters brought to mid-depths by ice-shelf overturning in the **runoff** experiment occupy large parts of the continental shelf (e.g., Figure 9a). Mixing over the upper 100–200 m resulting from winter brine rejection (e.g., Figure 9b) then brings this heat to the near-surface, where it limits sea ice growth in later seasons. The temperature elevation is very minor (<0.1°C) but enough to have an effect on sea ice—which may be amplified by other feedbacks in the ice/ocean system such as radiative heating. In the **increased** c_{fric} experiment, in which Thwaites overturning is relatively weak, this mid-depth warming at 100–400 m is mostly absent (Figure 9c). There is still a small surface warming signal due to there being some summer ice loss in this region (Figure 5f), though to a lesser extent than in **runoff**. In the **Thwaites only** experiment, there is again mid-depth warming (Figure 9e), but it is less persistent than in **runoff**. We therefore attribute the loss of summer sea ice in the **runoff** experiment to runoff-driven overturning under Thwaites ice shelf, and to a lesser extent under Pine Island ice shelf. Importantly, for similar freshwater volume fluxes, there appears to be a qualitatively different response in mid-depth ocean temperatures depending on the source.

We briefly note that the melt-overturning relationships in Figures 8a and 8b give regression slopes roughly twice of those found by Jourdain et al. (2017), and a far weaker linear relationship for Thwaites. However, it is a different model with different forcings, and their results are time-averaged across an ensemble of model parameters (whereas ours are monthly). Moreover our overturning calculation is distinct (though similar) to that study. Given that our model is of similar resolution, complexity and scale, we do not feel these differences diminish our findings.

4.2.2. Influence on Cavity Temperatures

While both ice-shelf melt and subglacial runoff lead to freshening, thermal effects differ since melting involves cooling due to latent heat. We therefore examine the role of water transformation under the ice shelves by considering temperature-salinity (T-S) diagrams under Pine Island and Thwaites for June 2011 (Figure 10), a month in which total Thwaites freshwater flux is very similar between the **runoff** and **increased Thwaites** c_{fric} experiments (Figure S7 in Supporting Information S1). While sea-ice reduction is largest in the summer months (cf. Figure 5), choosing a winter month removes water masses resulting from surface processes which complicate the diagram. Figure 10a overlays the T-S diagram from **baseline** on that of **runoff** and **increased** c_{fric}, restricted to Pine Island. Here a locus of points can be seen extending from (34.7 g/kg, 1°C) to (34.2 g/kg, −0.5°C) and approximately following a Gade line (blue line), indicative of water mass transformation due to ice-shelf melt (Gade, 1979). Little difference can be seen among the experiments.

Figure 10b compares the experiments under the region of Thwaites west of 106° W, the approximate location of runoff entry. In the **runoff** experiment there appears to be a freshening of water masses identified by a locus
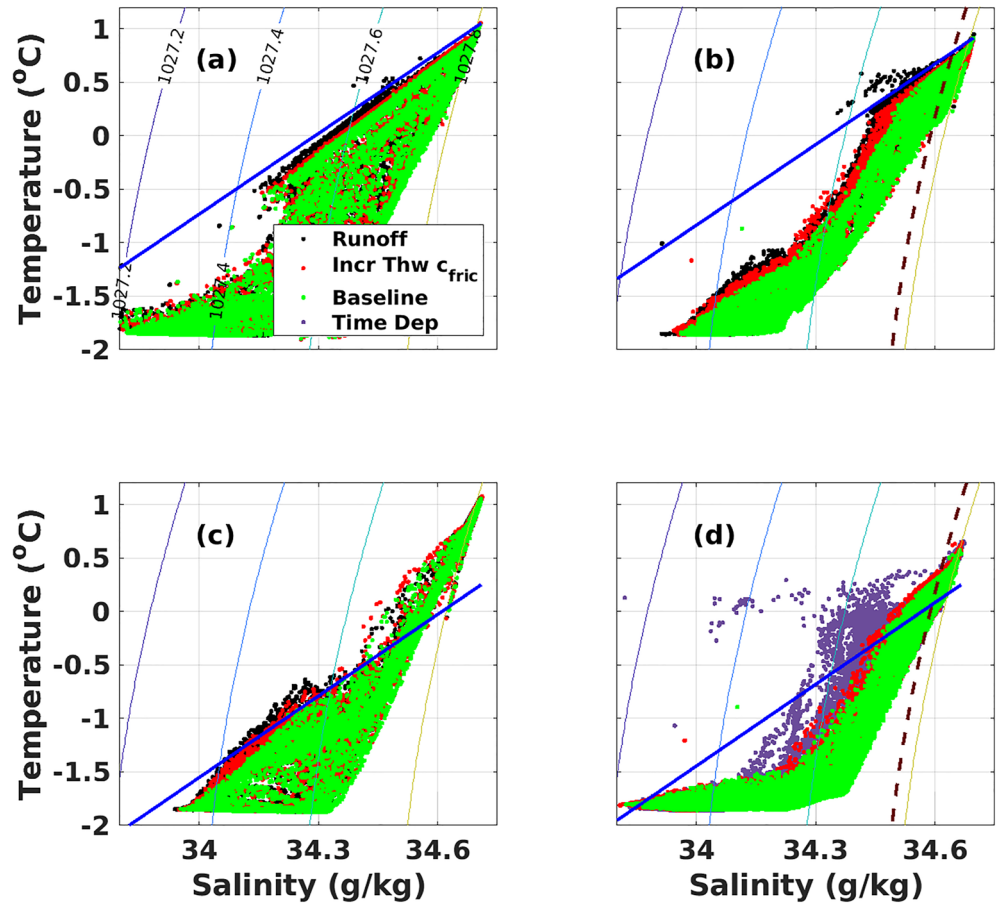
Figure 10. (a) Temperature-salinity diagrams for the **increased c_{fric}** (red), **runoff** (black), and **baseline** (green) experiments, limited to the Pine Island ice shelf cavity, in June 2011. Isolines of potential density in kg m^{-3} are shown (parula shading). The solid blue line has the approximate slope of the Gade line (Gade, 1979). Panel (b) similar to panel (a) but under the part of the Thwaites cavity to the east of the channel entering the cavity. Panel (c) similar to panel (b) but under the part of the Thwaites cavity to the west of the channel. The thick dashed density isoline indicates the density of the ocean cell where runoff is added. Panel (d) similar to panel (c) but for June 2013, with purple dots indicating output from the **time dependent runoff**, rather than the **runoff**, experiment.

of points above the blue Gade line originating at approximately salinity 34.6 g/kg and temperature 0.5°C. The locus originates at a potential density of ∼1,027.8 kg/m^3, that of the grounding line cell with the largest runoff flux. The feature is qualitatively similar to that seen in recent mooring data under Thwaites ice shelf (Davis et al., 2023) (their Figure 3d), which was also identified as subglacial runoff—although their hydrography analysis was far more localized than ours. Such a feature is absent from the part of Thwaites east of the runoff entry (Figure 10c). The effect is relatively minor, but could result in slightly warmed buoyant water masses that can cause upper-ocean warming on the continental shelf.

The effects are far more obvious in the **time dependent runoff** experiment. Figure 10d plots a similar T-S diagram for western Thwaites for June 2013, when runoff is at its peak. There is a strong freshening where runoff enters the cavity, identified by the locus of points extending leftward at ∼0°C. Due to subsequent transformation this then results in warmer waters, relative to the other experiments, at a range of densities. To put another way: since runoff freshens water without phase transformation, it does so without transforming along the relatively steep Gade line. Submarine melting of an ice shelf consumes latent heat, but for subglacial meltwater this heat is consumed beneath the ice sheet instead.

Still, this effective warming within Thwaites cavity alone does not explain the relative reduction in sea ice. However, the observations of Zheng et al. (2021) suggest that in the summer months, melt-freshened water exiting ice shelves can spread tens of kilometers or more away from the coast. Examination of our melt water

tracer (Figure S6 in Supporting Information S1) suggests similar behavior in our model. Thus it is plausible that, for a given density, runoff leads to warming, and that warming signal spreads across the shelf, giving rise to the mid-depth warming in Figure 6e. There may additionally be a positive feedback between ice loss and surface radiative heating.

4.3. Wider Significance

While the summer sea-ice reduction we see as a result of runoff (mean 3 cm, but up to ∼15 cm in places) is small compared to mean DJF sea ice thickness on the shelf (mean 70 cm), it is still significant. Reduction of sea ice is associated with stronger stratification, which can prevent convection and erosion of warm CDW. Sea ice cover is a major factor in biological productivity of the seasonal Pine Island and Amundsen Sea Polynyas, two of the most productive seasonal polynyas in Antarctica (Arrigo et al., 2012), and reduced sea ice thickness could modify productivity and carbon cycling.

The results are also significant because of how little is known about Antarctic subglacial hydrology. The experiments in this study simply represent different estimates of patterns of basal ice melt, and of spatiotemporal patterns of runoff. Steady runoff rates are derived based on estimates of geothermal flux, which could be over- or underestimates.

The results of our **time dependent runoff** experiment suggest that when runoff is episodic, the proportionate melt increase may be much smaller than the proportionate increase in runoff. As the runoff flux is expected to be the same in the long term, and hence the increase in runoff is inversely proportional to the period during which runoff occurs, this implies that the long-term impact of runoff on ice shelves is likely larger when runoff is sustained, rather than episodic. Meanwhile, episodic runoff has a strong impact on summer sea ice in our results. Observations of lake drainages (Hoffman et al., 2020; Malczyk et al., 2020; Smith et al., 2017) suggest episodic drainage does occur. If the Thwaites catchment were to transition from episodic to steady runoff in the future, this could have significant effects on ice-shelf melt and sea-ice variability.

The mechanism that we suggest above—that runoff leads to warmer sub-ice shelf water masses than an equivalent volume of submarine melt—is not specific to the Amundsen Sea Embayment. In other areas in Antarctica with strong subglacial activity and warm water under ice shelves (e.g., Dow et al., 2020; Gwyther et al., 2023), runoff likely has similar effects. As mentioned above, runoff effectively transfers latent heat from the ice sheet to the ocean by adding buoyancy without drawing heat content. With Antarctic-wide subglacial melt estimated to be ∼65 Gt/a (Pattyn, 2010), this is equivalent to 0.7 TW. In other words, an ocean model which seeks to reproduce fresh water flux from ice shelves without runoff will be deficient by this amount. While this is a small value relative to the estimated heat transported to the shelf from the deep ocean (∼20 TW, Palóczy et al., 2018), thermal signals associated with deep melting or runoff are likely to reach the upper ocean. Thus, subglacial runoff effectively represents a heat source not currently accounted for in ocean models.

5. Conclusions

We carry out a set of regional ocean simulations of the Amundsen Sea Embayment, some of which are forced by subglacial runoff with varying magnitudes and temporal character. Subglacial runoff is found to impact ice-shelf melt, both due to local and non-local effects. Episodic runoff leads to an increase in melt, but one that is not commensurate with the increase in runoff volume, based on expectations from steady simulations.

When normalizing for the input of fresh water to the ocean, the impact of runoff on sea ice is qualitatively different than that of increased ice-shelf melt. This sea-ice loss is coincident with an apparent warming under ice shelves. We propose this warming is driven by freshening due to runoff, and that the warming signal is brought to the surface, causing sea-ice reduction over the continental shelf in the summer months.

The results suggest that Antarctic runoff is a potentially important source of freshwater (and heat) not represented in regional and continental ocean models of Antarctica. Progress is impeded by lack of knowledge about Antarctica's subglacial environment. However, as direct observation of ice-shelf cavities and grounding lines increase (e.g., Begeman et al., 2018, 2020; Davis et al., 2023), this could lead to better quantification and deeper understanding of subglacial impact on the Southern Ocean.

Data Availability Statement

The MITgcm (mitgcm.org), checkpoint 67v was used for this study. The source is freely available for download (https://github.com/MITgcm/MITgcm). The zenodo archive https://doi.org/10.5281/zenodo.8157238 contains (a) all modified source code pertaining to the implementation of runoff in MITgcm (folder modified code/), (b) all experiment-specific code and inputs (input/ and expt_code/), and (c) all relevant model output (in output/).

References

Adusumilli, S., Fricker, H. A., Medley, B., Padman, L., & Siegfried, M. R. (2020). Interannual variations in meltwater input to the southern ocean from Antarctic ice shelves. *Nature Geoscience*, *13*(9), 616–620. https://doi.org/10.1038/s41561-020-0616-z

Arrigo, K. R., Lowry, K. E., & van Dijken, G. L. (2012). Annual changes in sea ice and phytoplankton in polynyas of the Amundsen Sea, Antarctica. *Deep Sea Research Part II: Topical Studies in Oceanography*, *71*, 5–15. https://doi.org/10.1016/j.dsr2.2012.03.006

Begeman, C. B., Tulaczyk, S., Padman, L., King, M., Siegfried, M. R., Hodson, T. O., & Fricker, H. A. (2020). Tidal pressurization of the ocean cavity near an Antarctic ice shelf grounding line. *Journal of Geophysical Research: Oceans*, *125*(4), e2019JC015562. https://doi.org/10.1029/2019JC015562

Begeman, C. B., Tulaczyk, S. M., Marsh, O. J., Mikucki, J. A., Stanton, T. P., Hodson, T. O., et al. (2018). Ocean stratification and low melt rates at the ross ice shelf grounding zone. *Journal of Geophysical Research: Oceans*, *123*(10), 7438–7452. https://doi.org/10.1029/2018JC013987

Bett, D. T., Holland, P. R., Naveira Garabato, A. C., Jenkins, A., Dutrieux, P., Kimura, S., & Fleming, A. (2020). The impact of the Amundsen Sea freshwater balance on ocean melting of the west Antarctic ice sheet. *Journal of Geophysical Research: Oceans*, *125*(9), e2020JC016305. https://doi.org/10.1029/2020JC016305

Brinkerhoff, D., Aschwanden, A., & Fahnestock, M. (2021). Constraining subglacial processes from surface velocity observations using surrogate-based bayesian inference. *Journal of Glaciology*, *67*(263), 385–403. https://doi.org/10.1017/jog.2020.112

Colgan, W., MacGregor, J. A., Mankoff, K. D., Haagenson, R., Rajaram, H., Martos, Y. M., et al. (2021). Topographic correction of geothermal heat flux in Greenland and Antarctica. *Journal of Geophysical Research: Earth Surface*, *126*(2), e05598. https://doi.org/10.1029/2020JF005598

Cowton, T., Slater, D., Sole, A., Goldberg, D., & Nienow, P. (2015). Modeling the impact of glacial runoff on fjord circulation and submarine melt rate using a new subgrid-scale parameterization for glacial plumes. *Journal of Geophysical Research: Oceans*, *120*(2), 796–812. https://doi.org/10.1002/2014JC010324

Cowton, T., Sole, A., Nienow, P., Slater, D., Wilton, D., & Hanna, E. (2016). Controls on the transport of oceanic heat to kangerdlugssuaq glacier, east Greenland. *Journal of Glaciology*, *62*(236), 1167–1180. https://doi.org/10.1017/jog.2016.117

Cuffey, K., & Paterson, W. S. B. (2010). *The physics of glaciers* (4th ed.). Butterworth Heinemann.

Dansereau, V., Heimbach, P., & Losch, M. (2014). Simulation of subice shelf melt rates in a general circulation model: Velocity-dependent transfer and the role of friction. *Journal of Geophysical Research: Oceans*, *119*(3), 1765–1790. https://doi.org/10.1002/2013JC008846

Davis, P. E., Nicholls, K. W., Holland, D. M., Schmidt, B. E., Washam, P., Riverman, K. L., et al. (2023). Suppressed basal melting in the eastern Thwaites glacier grounding zone. *Nature*, *614*(7948), 479–485. https://doi.org/10.1038/s41586-022-05586-0

Depoorter, M. A., Bamber, J. L., Griggs, J. A., Lenaerts, J. T. M., Ligtenberg, S. R. M., van den Broeke, M. R., & Moholdt, G. (2013). Calving fluxes and basal melt rates of Antarctic ice shelves. *Nature*, *502*(7469), 89–92. https://doi.org/10.1038/nature12567

Dow, C., McCormack, F., Young, D., Greenbaum, J., Roberts, J., & Blankenship, D. (2020). Totten glacier subglacial hydrology determined from geophysics and modeling. *Earth and Planetary Science Letters*, *531*, 115961. https://doi.org/10.1016/j.epsl.2019.115961

Drews, R., Pattyn, F., Hewitt, I. J., Ng, F. S. L., Berger, S., Matsuoka, K., et al. (2017). Actively evolving subglacial conduits and eskers initiate ice shelf channels at an Antarctic grounding line. *Nature Communications*, *8*(1), 15228. https://doi.org/10.1038/ncomms15228

Favier, L., Durand, G., Cornford, S. L., Gudmundsson, G. H., Gagliardini, O., Gillet-Chaulet, F., et al. (2014). Retreat of Pine Island Glacier controlled by marine ice-sheet instability. *Nature Climate Change*, *4*(2), 117–121. https://doi.org/10.1038/nclimate2094

Gade, H. G. (1979). Melting of ice in sea water: A primitive model with application to the Antarctic ice shelf and icebergs. *Journal of Physical Oceanography*, *9*(1), 189–198. https://doi.org/10.1175/1520-0485(1979)009<0189:MOIISW>2.0.CO;2

Goldberg, D. N., & Holland, P. (2022). The relative impacts of initialisation and climate forcing in coupled ice sheet-ocean modelling application to Pope, Smith and Kohler glaciers. *Journal of Geophysical Research: Earth Surface*, *127*(5), e2021JF006570. https://doi.org/10.1029/2021JF006570

Goldberg, D. N., Gourmelen, N., Kimura, S., Millan, R., & Snow, K. (2019). How accurately should we model ice shelf melt rates? *Geophysical Research Letters*, *46*(1), 189–199. https://doi.org/10.1029/2018GL080383

Goldberg, D. N., & Heimbach, P. (2013). Parameter and state estimation with a time-dependent adjoint marine ice sheet model. *The Cryosphere*, *7*(6), 1659–1678. https://doi.org/10.5194/tc-7-1659-2013

Gwyther, D. E., Dow, C. F., Jendersie, S., Gourmelen, N., & Galton-Fenzi, B. K. (2023). Subglacial freshwater drainage increases simulated basal melt of the Totten ice shelf. *Geophysical Research Letters*, *50*(12), e2023GL103765. https://doi.org/10.1029/2023GL103765

Hager, A. O., Hoffman, M. J., Price, S. F., & Schroeder, D. M. (2022). Persistent, extensive channelized drainage modeled beneath Thwaites glacier, west Antarctica. *The Cryosphere*, *16*(9), 3575–3599. https://doi.org/10.5194/tc-16-3575-2022

Hoffman, A. O., Christianson, K., Shapero, D., Smith, B. E., & Joughin, I. (2020). Brief communication: Heterogenous thinning and subglacial lake activity on Thwaites glacier, west Antarctica. *The Cryosphere*, *14*(12), 4603–4609. https://doi.org/10.5194/tc-14-4603-2020

Holland, P. R., Bevan, S. L., & Luckman, A. J. (2023). Strong ocean melting feedback during the recent retreat of Thwaites glacier. *Geophysical Research Letters*, *50*(8), e2023GL103088. https://doi.org/10.1029/2023GL103088

Jenkins, A. (2011). Convection-driven melting near the grounding lines of ice shelves and tidewater glaciers. *Journal of Physical Oceanography*, *41*(12), 2279–2294. https://doi.org/10.1175/JPO-D-11-03.1

Joughin, I., Smith, B. E., & Medley, B. (2014). Marine ice sheet collapse potentially under way for the Thwaites glacier basin, West Antarctica. *Science*, *344*(6185), 735–738. https://doi.org/10.1126/science.1249055

Joughin, I., Tulaczyk, S., Bamber, J. L., Blankenship, D., Holt, J. W., Scambos, T., & Vaughan, D. G. (2009). Basal conditions for Pine Island and Thwaites glaciers, West Antarctica, determined using satellite and airborne data. *Journal of Glaciology*, *55*(190), 245–257. https://doi.org/10.3189/002214309788608705

Jourdain, N. C., Mathiot, P., Merino, N., Durand, G., Le Sommer, J., Spence, P., et al. (2017). Ocean circulation and sea-ice thinning induced by melting ice shelves in the a Mundsen sea. *Journal of Geophysical Research: Oceans*, *122*(3), 2550–2573. https://doi.org/10.1002/2016JC012509

Kimura, S., Jenkins, A., Regan, H., Holland, P. R., Assmann, K. M., Whitt, D. B., et al. (2017). Oceanographic controls on the variability of ice-shelf basal melting and circulation of glacial meltwater in the Amundsen Sea Embayment, Antarctica. *Journal of Geophysical Research: Oceans*, *122*(12), 10131–10155. https://doi.org/10.1002/2017JC012926

Le Brocq, A. M., Payne, A. J., Siegert, M. J., & Alley, R. B. (2009). A subglacial water-flow model for West Antarctica. *Journal of Glaciology*, *55*(193), 879–888. https://doi.org/10.3189/002214309790152564

Le Brocq, A. M., Ross, N., Griggs, J. A., Bingham, R. G., Corr, H. F., Ferraccioli, F., et al. (2013). Evidence from ice shelves for channelized meltwater flow beneath the Antarctic ice sheet. *Nature Geoscience*, *6*(11), 945–948. https://doi.org/10.1038/ngeo1977

Locarnini, M., Mishonov, A., Baranova, O., Boyer, T., Zweng, M., Garcia, H., et al. (2018). *World ocean atlas 2018, volume 1: Temperature* [Report]. NOAA Atlas. Retrieved from https://archimer.ifremer.fr/doc/00651/76338/

Losch, M. (2008). Modeling ice shelf cavities in a z coordinate ocean general circulation model. *Journal of Geophysical Research*, *113*(C8), C08043. https://doi.org/10.1029/2007JC004368

Losch, M., Menemenlis, D., Campin, J.-M., Heimbach, P., & Hill, C. (2010). On the formulation of sea-ice models. Part 1: Effects of different solver implementations and parameterizations. *Ocean Modelling*, *33*(1), 129–144. https://doi.org/10.1016/j.ocemod.2009.12.008

Malczyk, G., Gourmelen, N., Goldberg, D., Wuite, J., & Nagler, T. (2020). Repeat subglacial lake drainage and filling beneath Thwaites glacier. *Geophysical Research Letters*, *47*(23), e2020GL089658. https://doi.org/10.1029/2020GL089658

Marshall, J., Hill, C., Perelman, L., & Adcroft, A. (1997). Hydrostatic, quasi-hydrostatic, and nonhydrostatic ocean modeling. *Journal of Geophysical Research*, *102*(C3), 5733–5752. https://doi.org/10.1029/96JC02776

Martos, Y. M., Catalán, M., Jordan, T. A., Golynsky, A., Golynsky, D., Eagles, G., & Vaughan, D. G. (2017). Heat flux distribution of Antarctica unveiled. *Geophysical Research Letters*, *44*(22), 11147–11426. https://doi.org/10.1002/2017GL075609

Mathiot, P., Jenkins, A., Harris, C., & Madec, G. (2017). Explicit representation and parametrised impacts of under ice shelf seas in the z coordinate ocean model NEMO 3.6. *Geoscientific Model Development*, *10*(7), 2849–2874. https://doi.org/10.5194/gmd-10-2849-2017

Merino, N., Le Sommer, J., Durand, G., Jourdain, N. C., Madec, G., Mathiot, P., & Tournadre, J. (2016). Antarctic icebergs melt over the southern ocean: Climatology and impact on sea ice. *Ocean Modelling*, *104*, 99–110. https://doi.org/10.1016/j.ocemod.2016.05.001

Mernild, S., Howat, I. M., Ahn, Y., Liston, G. E., Steffen, K., Jakobsen, B. H., et al. (2010a). Freshwater flux to Sermilik Fjord, SE Greenland. *The Cryosphere*, *4*(4), 453–465. https://doi.org/10.5194/tc-4-453-2010

Mernild, S., Liston, G. E., Steffen, K., & Chylek, P. (2010b). Meltwater flux and runoff modeling in the ablation area of Jakobshavn Isbræ, West Greenland. *Journal of Glaciology*, *56*(195), 20–32. https://doi.org/10.3189/002214310791190794

Morlighem, M., Rignot, E., Binder, T., Blankenship, D., Drews, R., Eagles, G., et al. (2020). Deep glacial troughs and stabilizing ridges unveiled beneath the margins of the Antarctic ice sheet. *Nature Geoscience*, *13*(2), 132–137. https://doi.org/10.1038/s41561-019-0510-8

Motyka, R. J., Dryer, W. P., Amundson, J., Truffer, M., & Fahnestock, M. (2013). Rapid submarine melting driven by subglacial discharge, leconte glacier, Alaska. *Geophysical Research Letters*, *40*(19), 5153–5158. https://doi.org/10.1002/grl.51011

Nakayama, Y., Cai, C., & Seroussi, H. (2021). Impact of subglacial freshwater discharge on Pine Island ice shelf. *Geophysical Research Letters*, *48*(18), e93923. https://doi.org/10.1029/2021GL093923

Naughten, K. A., De Rydt, J., Rosier, S. H., Jenkins, A., Holland, P. R., & Ridley, J. K. (2021). Two-timescale response of a large Antarctic ice shelf to climate change. *Nature Communications*, *12*(1), 1–10. https://doi.org/10.1038/s41467-021-22259-0

Naughten, K. A., Holland, P. R., Dutrieux, P., Kimura, S., Bett, D. T., & Jenkins, A. (2022). Simulated twentieth-century ocean warming in the Amundsen Sea, West Antarctica. *Geophysical Research Letters*, *49*(5), e94566. https://doi.org/10.1029/2021GL094566

Nienow, P., Sole, A., Slater, D. A., & Cowton, T. (2017). Recent advances in our understanding of the role of meltwater in the Greenland ice sheet system. *Current Climate Change Reports*, *3*(4), 330–344. https://doi.org/10.1007/s40641-017-0083-9

Palóczy, A., Gille, S. T., & McClean, J. L. (2018). Oceanic heat delivery to the Antarctic continental shelf: Large-scale, low-frequency variability. *Journal of Geophysical Research: Oceans*, *123*(11), 7678–7701. https://doi.org/10.1029/2018JC014345

Pattyn, F. (2010). Antarctic subglacial conditions inferred from a hybrid ice sheet/ice stream model. *Earth and Planetary Science Letters*, *295*(3–4), 451–461. https://doi.org/10.1016/j.epsl.2010.04.025

Rignot, E., Jacobs, S., Mouginot, J., & Scheuchl, B. (2013). Ice-shelf melting around Antarctica. *Science*, *341*(6143), 266–270. https://doi.org/10.1126/science.1235798

Rignot, E., Mouginot, J., & Scheuchl, B. (2011). Ice flow of the Antarctic ice sheet. *Science*, *333*(6048), 1427–1430. https://doi.org/10.1126/science.1208336

Schroeder, D. M., Blankenship, D. D., & Young, D. A. (2013). Evidence for a water system transition beneath Thwaites glacier, west Antarctica. *Proceedings of the National Academy of Sciences*, *110*(30), 12225–12228. https://doi.org/10.1073/pnas.1302828110

Seroussi, H., Nakayama, Y., Larour, E., Menemenlis, D., Morlighem, M., Rignot, E., & Khazendar, A. (2017). Continued retreat of Thwaites glacier, west Antarctica, controlled by bed topography and ocean circulation. *Geophysical Research Letters*, *44*(12), 6191–6199. https://doi.org/10.1002/2017GL072910

Silvano, A., Rintoul, S. R., Peña-Molino, B., Hobbs, W. R., van Wijk, E., Aoki, S., et al. (2018). Freshening by glacial meltwater enhances melting of ice shelves and reduces formation of Antarctic bottom water. *Science Advances*, *4*(4), eaap9467. https://doi.org/10.1126/sciadv.aap9467

Slater, D., Nienow, P., Cowton, T., Goldberg, D., & Sole, A. (2015). Effect of near-terminus subglacial hydrology on tidewater glacier submarine melt rates. *Geophysical Research Letters*, *42*(8), 2861–2868. https://doi.org/10.1002/2014GL062494

Slater, D., Straneo, F., Das, S., Richards, C., Wagner, T., & Nienow, P. (2018). Localized plumes drive front-wide ocean melting of a Greenlandic tidewater glacier. *Geophysical Research Letters*, *45*(22), 12–350. https://doi.org/10.1029/2018GL080763

Smith, B. E., Gourmelen, N., Huth, A., & Joughin, I. (2017). Connected subglacial lake drainage beneath Thwaites glacier, west Antarctica. *The Cryosphere*, *11*(1), 451–467. https://doi.org/10.5194/tc-11-451-2017

Van Lieffringe, B., & Pattyn, F. (2013). Using ice-flow models to evaluate potential sites of million year-old ice in Antarctica. *Climate of the Past Discussions*, *9*(3), 2335–2345. https://doi.org/10.5194/cp-9-2335-2013

Verdy, A., & Mazloff, M. R. (2017). A data assimilating model for estimating Southern Ocean biogeochemistry. *Journal of Geophysical Research: Oceans*, *122*(9), 6968–6988. https://doi.org/10.1002/2016JC012650

Xu, Y., Rignot, E., Fenty, I., Menemenlis, D., & Flexas, M. M. (2013). Subaqueous melting of store glacier, west Greenland from three-dimensional, high-resolution numerical modeling and ocean observations. *Geophysical Research Letters*, *40*(17), 4648–4653. https://doi.org/10.1002/grl.50825

Yager, P. L., Sherrell, R. M., Stammerjohn, S. E., Alderkamp, A.-C., Schofield, O., Abrahamsen, E. P., et al. (2012). Aspire: The Amundsen Sea polynya international research expedition. *Oceanography*, *25*(3), 40–53. https://doi.org/10.5670/oceanog.2012.73

Yoon, S.-T., Lee, W. S., Nam, S., Lee, C.-K., Yun, S., Heywood, K., et al. (2022). Ice front retreat reconfigures meltwater-driven gyres modulating ocean heat delivery to an Antarctic ice shelf. *Nature Communications*, *13*(1), 1–8. https://doi.org/10.1038/s41467-022-27968-8

Zheng, Y., Heywood, K. J., Webber, B. G., Stevens, D. P., Biddle, L. C., Boehme, L., & Loose, B. (2021). Winter seal-based observations reveal glacial meltwater surfacing in the southeastern Amundsen Sea. *Communications Earth & Environment*, *2*(1), 1–9. https://doi.org/10.1038/s43247-021-00111-z

Zweng, M., Reagan, J., Seidov, D., Boyer, T., Locarnini, M., Garcia, H., et al. (2019). *World ocean atlas 2018, volume 2: Salinity*. [Report]. NOAA Atlas. https://archimer.ifremer.fr/doc/00651/76339/